Mon. Not. R. Astron. Soc. **367,** 1629–1640 (2006) doi:10.1111/j.1365-2966.2006.10062.x

Shapes and sizes of voids in the Lambda cold dark matter universe: excursion set approach

Sergei Shandarin,[1,3⋆] Hume A. Feldman,[1⋆] Katrin Heitmann[2⋆] and Salman Habib[3⋆]

[1]*Department of Physics & Astronomy, University of Kansas, Lawrence, KS 66045, USA*
[2]*ISR-1, The University of California, Los Alamos National Laboratory, Los Alamos, NM 87545, USA*
[3]*T-8, The University of California, Los Alamos National Laboratory, Los Alamos, NM 87545, USA*

Accepted 2006 January 10. Received 2005 December 22; in original form 2005 September 30

ABSTRACT

We study the global distribution and morphology of dark matter voids in a Lambda cold dark matter (ΛCDM) universe using density fields generated by N-body simulations. Voids are defined as isolated regions of the low-density excursion set specified via density thresholds, the density thresholds being quantified by the corresponding filling factors, i.e. the fraction of the total volume in the excursion set. Our work encompasses a systematic investigation of the void volume function, the volume fraction in voids and the fitting of voids to corresponding ellipsoids and spheres. We emphasize the relevance of the percolation threshold to the void volume statistics of the density field in the high redshift, Gaussian random field regime as well as in the present epoch. By using measures such as the Inverse Porosity, we characterize the quality of ellipsoidal fits to voids, finding that such fits are a poor representation of the larger voids that dominate the volume of the void excursion set.

Key words: cosmology: theory – dark matter – large-scale structure of Universe.

1 INTRODUCTION

The detailed distribution of mass in the Universe is only now being fully revealed by large-scale astronomical surveys. Consequently, in the last decade or so, a great deal of effort has gone into detailed studies of the high-density regions, in particular the progenitors of galaxies and clusters of galaxies. The density profiles, merging history, substructure and many other features have been increasingly accurately modelled, simulated and analysed. This is not surprising because these are precisely the places where most 'action' occurs: the first objects, galaxy formation and merging, X-rays, gravitational lensing, etc.

But even the lower density, ostensibly 'quiet' regions of the Universe are of significant interest: recent studies indicate a discrepancy between observations and theory in low- and medium-density regions which are naturally associated with voids and filaments or walls, respectively. Simulations show that dark matter haloes in voids are capable of developing into void objects observable as (dwarf) galaxies. However, the morphology–density correlation, so natural in the biased galaxy formation scenario, seems to be in contrast to what is observed. Despite a fairly long history of studies (see, e.g. Gregory & Thompson 1978; Zel'dovich, Einasto & Shandarin 1982; Rood 1988), the problems of void phenomenology remain serious enough for Peebles (2001) to conclude: 'The apparent inconsistency between the theory and observations of voids is striking enough to be classified as a crisis of the cold dark matter (CDM) model.'

The study of low- and medium-density regions is demanding from both the observational and modelling perspectives. From the point of view of observations, large contiguous regions need to be surveyed in sufficient depth and spectra, colours and morphology information for the surveyed galaxies obtained. Fortunately, the observational impediment is coming to an end: the 2dF redshift survey (Colless et al. 2001) has been completed and the data released, and the Sloan Digital Sky Survey (SDSS) has begun to release large volumes of data (Adelman-McCarthy et al. 2006). As a result, valuable information on the luminosity function, colours, concentration and other attributes of galaxies in voids and void walls have been obtained (Rojas et al. 2004; Hoyle et al. 2005). The interpretation of these results, however, relied heavily on the purely phenomenological VOIDFINDER algorithm of Hoyle & Vogeley (2002) (see also El-Ad & Piran 1997; Benson et al. 2003) that assumes voids to be nearly spherical and also depends on ad hoc parameters such as the criteria for 'void' and 'wall' galaxies first introduced by El-Ad & Piran (1997). As a cautionary remark, the relation of the above observational results to the physical processes in voids and void walls does not seem to be trivial.

Observational studies of voids and superclusters searching for various correlations between properties of galaxies and their environment often do not take into account the fact that some galaxies may travel distances comparable to the sizes of voids (up to roughly half of the radius of a spherical void, as estimated in Appendix A), and are then artificially shifted further by the observationally

⋆E-mail: sergei@ku.edu (SS); feldman@ku.edu (HAF); heitmann@lanl.gov (KH); habib@lanl.gov (SH)

© 2006 The Authors. Journal compilation © 2006 RAS

Downloaded from https://academic.oup.com/mnras/article-abstract/367/4/1629/1747190/ by guest on 07 October 2019

unavoidable mapping into redshift space. Therefore, the environment where the galaxies were originally formed might well be quite different from the one where they are ostensibly observed: The physical processes that govern the observed properties of galaxies in voids and in void walls certainly operate in physical space and not in redshift space.

Additionally, theoretical models of voids remain oversimplified; the assumption that voids have close to spherical shapes is often the basis of theoretical and observational studies (Kauffmann & Fairall 1991; Dubinski et al. 1993; Ryden 1995; Amendola, Frieman & Waga 1999; Goldberg & Vogeley 2004). Some algorithms formally allow non-sphericity but in a quite limited form (see e.g. Aikio & Mähönen 1998). This prejudice is partly based on a result due to Icke (1984) who noted that by changing the sign in the solution for the collapse of a uniform ellipsoidal enhancement (Lin, Mestel & Shu 1965) one can describe the evolution of an ellipsoidal void. He showed that the asphericities of an isolated ellipsoidal underdense perturbation 'tend to disappear' as the void becomes bigger. Following this, many theoretical studies of void evolution have taken the spherical model for granted. Icke's conclusion, however, was based only on inequalities regarding the relative accelerations along principal axes of the ellipsoid. He did not integrate the equations, and therefore the evolution of the ratios of the principal axes remained unknown. Bertschinger (1985), who studied the evolution of an isolated uniform ellipsoidal void numerically, confirmed the effect found by Icke. However, quantitatively his result was not very impressive: an initially oblate ellipsoid with axis ratio $c_i/a_i = 0.5$ and density $\rho_i = 0.9\bar{\rho}(t_i)(\delta_i = -0.1)$ evolved to a more spherical ellipsoid with $c_\mathrm{f}/a_\mathrm{f} = 0.722$ when the density inside the ellipsoid dropped to $\rho_\mathrm{f} = 0.04\bar{\rho}(t_\mathrm{f})(\delta_\mathrm{f} = -0.96)$ after the Einstein–de Sitter universe had expanded to 162 times its initial size. One can hardly expect that a void can evolve for such a long time without being seriously disturbed by its neighbours. For instance, as predicted by the adhesion approximation, the shape of voids is likely to be affected by violent interactions with adjoining superclusters and voids resulting in the growth of some voids at the expense of other voids (Kofman et al. 1992; Sahni, Sathyaprakash & Shandarin 1994). Another caveat regarding Icke's model is the negligence of external shear. Eisenstein & Loeb (1995) have emphasized that even in the case of the collapsing ellipsoid, the shape change is primarily induced by the external shear and not by the initial triaxiality of the objects. Due to their low internal density, it is clear that the external shear must play an even stronger role in the case of voids. In any case, the issue of dynamical evolution of voids appears to be unsettled and requires further study.

From the point of view of detailed modelling, voids require large simulation volumes, while at the same time, high mass resolution is necessary to track the smaller dark matter haloes that populate the voids. In addition, hydrodynamics, feedback, star formation, etc. need to be modelled adequately to understand galaxy formation in the void complex. It is worth noting here that theory (Kofman et al. 1992; Sahni et al. 1994) as well as some N-body simulations (Kofman et al. 1992; Dubinski et al. 1993; van de Weygaert & van Kampen 1993; Gottlöber et al. 2003) indicates that both superclusters and voids have non-trivial substructure and complicated internal dynamics. As an example, very complex substructures have been detected and studied in dark matter superclusters (Shandarin, Sheth & Sahni 2004) and voids by the Virgo consortium utilizing N-body simulations (Jenkins et al. 1998).

The problems outlined above require a more systematic study of voids – of their morphology and topology, dynamics and internal structure. Assuming that the low dark matter density regions are closely related to observational voids, we concentrate here on the most basic global properties: their sizes and shapes. We study the dark matter mass distribution in real space obtained from N-body simulations of the ΛCDM model. Although the mass distribution in real space cannot be measured directly, it controls the dynamics, as well as other properties of voids.

It is worth stressing that there is no commonly accepted definition of a void. Here, we employ the underdense excursion set approach: voids are defined as individual regions where the density contrast is below a certain threshold δ_c. The boundaries of the voids are therefore closed surfaces of constant density contrast δ_c. The advantages of this definition include (i) simplicity, (ii) a clear uniform definition of void boundaries[1] allowing the study of shapes and sizes and (iii) symmetry with the common definition of superclusters as regions with densities above a specified density threshold. We do not preselect any particular threshold but rather study the transformation of voids as the threshold is raised from low to high values. As in other definitions of voids, we also assume a certain smoothing procedure for the density field which we take here to be a uniform Gaussian filter. This allows a continuous transition to a Gaussian density field if the scale of the filter window is taken to be sufficiently large.

As further discussed below, one of the consequences of this definition is the associated percolation transition: at thresholds above a certain value, the largest void spans the entire volume and quickly becomes the dominant structure in the underdense excursion set. At the threshold corresponding approximately to the percolation transition, the individual voids reach their largest sizes and volumes. We will quantitatively study the shapes and sizes of underdense regions at these thresholds.

Although we do not attempt to review the entire body of work on voids, we would like to emphasize that many other definitions of voids have been previously suggested (Kirshner et al. 1981; Kauffmann & Fairall 1991; Sahni et al. 1994; El-Ad & Piran 1997; Aikio & Mähönen 1998; Plionis & Basilakos 2002; Benson et al. 2003; Colberg et al. 2005). All of them are claimed to be in agreement with visual impressions of observed data and N-body simulations. While 'visual impression' pertains more to the expertise of psychology rather than physics or astronomy, in general these various definitions agree at least on one basic principle: dynamically, voids must be closely related to the underdense regions. Often, the algorithms finding voids are designed to suppress narrow tunnels between two fat voids (see e.g. Kauffmann & Fairall 1991; Colberg et al. 2005). This inevitably involves additional ad hoc parameters describing which tunnel is narrow and which is not. In addition, there are attempts to incorporate some concepts of theoretical dynamical models into the construction of voids (see e.g. Dubinski et al. 1993; van de Weygaert & van Kampen 1993; Benson et al. 2003; Colberg et al. 2005); in practice, this is essentially the spherical model of void evolution.

In this paper, we develop an unbiased (i.e. without any theoretical or aesthetic or other ad hoc assumptions) technique that is able to identify voids and then quantify – at least crudely – their shapes. The only 'arbitrary' parameter is the scale of smoothing of the dark matter density field. We emphasize that in N-body simulations, particles are merely tracers of the density field, and their masses have neither physical nor astronomical meaning. The particle mass is completely determined by computational limitations which put an upper bound

[1] Numerous void finding algorithms often define different parts of the boundary surface by different conditions.

Downloaded from https://academic.oup.com/mnras/article-abstract/367/4/1629/1747190/ by guest on 07 October 2019

on the number of particles. Therefore, in contrast to galaxy distributions in redshift catalogues, the discreteness of density fields obtained from N-body simulations is an artefact of the simulation technique and must be suppressed. Smoothing represents an attempt to approximately recover the underlying dark matter density field from a discrete particle distribution by suppressing the underlying shot noise. In this study, the smoothing filter is taken to be a uniform Gaussian window [$\propto \exp(-r^2/2R_f^2)$]. Obviously, this is not an optimal smoothing method, and we are planning to improve this part of the technique in future work. A particularly promising method of constructing the density field from point-like distributions obtained in redshift surveys and N-body simulations is based on Delaunay tesselations (Schaap & van de Weygaert 2000; van de Weygaert 2002). Density fields reconstructed in this manner appear to preserve anisotropic features, and therefore may have some advantages over conventional 'Cloud-In-Cell' (CIC) techniques followed by an isotropic smoothing, as performed here.

As stated earlier, we define voids as isolated regions of the low-density excursion set specified by a density threshold: $\delta \equiv \delta\rho/\rho < \delta_c$. This definition is significantly different from the many definitions used in the literature in one particular sense. It defines the boundary of the void explicitly and unambiguously. In contrast, most other studies define a void as an underdense region surrounding the minimum of the density field (e.g. van de Weygaert & van Kampen 1993). The boundary may remain unspecified exactly (e.g. Gottlöber et al. 2003; Sheth & van de Weygaert 2004) or be constructed (e.g. Kauffmann & Fairall 1991; Aikio & Mähönen 1998). Though in both cases, it is implied that the boundary approximately corresponds to the surface of constant density, various exceptions from the rule are usually allowed.

In our systematic study of the void excursion sets at a large number of density thresholds, we identify a particular threshold when the voids are the largest by volume. This threshold is just below the percolation threshold ($\delta \leqslant \delta_c$) where voids merge with each other and form a single percolating void that spans the entire volume of the simulation (Sheth et al. 2003; Shandarin et al. 2004). The percolating void itself does not have a well-defined volume and has a very complicated geometry and topology; however, it possesses interesting scaling properties. We show that the individual regions of the underdense excursion set do not have spherical shapes: the mean ratio of the smallest to largest axis is about 0.45 more or less independently of the void volume. In addition, using quantitative measures such as the Inverse Porosity, we investigate to what extent ellipsoidal and spherical volumes can be used as good approximations for realistic void shapes (as given by our definition). We conclude that while such an approach may work for small voids, it is a poor approximation for the larger voids which dominate the volume of the void excursion set.

This article is organized as follows. In Section 2, we describe the N-body simulations used in this study. In Section 3, we define the void volume function, the number of voids of a given volume and the void volume fraction. In Section 4, we briefly discuss voids in a cosmologically relevant Gaussian random field and then, in Section 5, the voids resulting from N-body simulations of the ΛCDM model. In Section 6, we show how to approximate voids by ellipsoids and define the voids' Inverse Porosity. In Section 7, we define and quantify the sphericity of voids and discuss the statistical distribution of void shapes. In Section 8, we discuss the shapes of the voids in the simulations. Specifically, we discuss the mean Sphericity and Inverse Porosity (Section 8.1) and their distribution functions (Section 8.2) as found from the simulations. We summarize and conclude in Section 9.

2 *N*-BODY SIMULATIONS

The dark matter density field at early times is taken to be a Gaussian random field, specified completely in real space by its two-point statistics and in k-space, by the primordial fluctuation power spectrum $P(k)$, typically assumed to be a power law. At later times, the density field on the length scales of interest here is non-linear and non-Gaussian. Accurate evolution of the initial density field on these scales requires the application of numerical N-body methods.

Our primary interest here is in the shapes and sizes of void regions and not in studying the detailed dynamics and galaxy formation within. Since the relevant void sizes are on the scales of tens of Mpc, a simulation box of 256 h^{-1} Mpc (h is the Hubble parameter in units of 100 km s^{-1} Mpc^{-1}) provides an adequate total volume for the gathering of void statistics. A void is defined operationally by considering a smoothed density field with a smoothing scale of the order of 1 Mpc; it follows that for the studies reported here, force resolution demands are modest and easily met. Similarly, as we are not interested in the details of the density field interior to the void, the mass resolution required is also easily attained. N-body simulations with $N_p = 256^3$ particles corresponding to an individual particle mass of $1.227 \times 10^{11}\,\mathrm{M}_\odot$ are sufficient for the task.

Given the requirements above, a particle–mesh (PM) code is completely adequate. The simulations were performed using the parallel PM code-suite MC^2 (Mesh-based Cosmology Code), one of the codes used recently in an extensive test of cosmological large-scale structure simulations (Heitmann et al. 2005). The cosmological parameters were taken to be $\Omega_m = 0.314$ (where Ω_m includes both dark matter and baryons), $\Omega_b = 0.044$, $\Omega_\Lambda = 0.686$, $H_0 = 71$ km s^{-1} Mpc^{-1}, $\sigma_8 = 0.84$ and $n = 0.99$. These values are in concordance with the *Wilkinson Microwave Anisotropy Probe* (*WMAP*) measurement (Spergel et al. 2003). The matter transfer function was generated using the fits from Klypin & Holtzman (1997), the initial redshift was $z_{in} = 50$, and periodic boundary conditions were used.

3 VOID VOLUME FUNCTION AND VOLUME FRACTION

The dark matter density field on a grid is obtained from the spatial N-body particle distribution by applying the CIC method followed by smoothing with a Gaussian filter. Using this smoothed density field, we define a void as an individual region bounded by one or more closed surfaces. Thus, a void is identified as a set of grid sites with density contrast [$\delta \equiv (\rho - \bar{\rho})/\bar{\rho}$, where ρ and $\bar{\rho}$ are the density and mean density, respectively] below a selected threshold ($\delta \leqslant \delta_c$) and satisfying a neighbouring criterion consisting of two conditions. First, that the six closest sites are the immediate neighbours of the selected site and, secondly, that the immediate neighbours of every neighbour are also the neighbours of the site. The volume of each void is estimated using the number of its sites multiplied by the volume associated with the grid cell. All voids at a given density threshold make up the void excursion set. We quantify the density thresholds by the corresponding filling factors (FF), i.e. the fraction of the total volume in the excursion set.

The void volume function $n(V)$ gives the number[2] of voids having the given volume V

$$\mathrm{d}N = n(V)\,\mathrm{d}V. \tag{1}$$

[2] It should be noted that in the discussion below, the number of voids quoted is for the particular simulation box volume $V_{box} = 256^3$ $(h^{-1}$ Mpc$)^3$ and the particular bin sizes: $\Delta V/V = 1/\sqrt{2}$. The statistical significance of the results can be directly assessed using the total number of voids in every bin.

Downloaded from https://academic.oup.com/mnras/article-abstract/367/4/1629/1747190/ by guest on 07 October 2019

The behaviour of the void volume function is shown in the left-hand panels of Fig. 1 for a density field at a very early epoch $z = 150$ – essentially a Gaussian field – whereas Figs 3 and 4 show the void volume function for evolved non-linear dark matter density fields. These results will be discussed in detail in the following sections.

The volume fraction in voids, $\nu(V)$, specifies the amount of volume in voids of a given volume V, following directly from the definition of the void volume function $n(V)$

$$\nu(V)\,\mathrm{d}V = \frac{V}{V_t} n(V)\,\mathrm{d}V, \tag{2}$$

where V_t is the volume of the simulation box. We stress that the largest void must be excluded from this statistic because of its peculiar properties around the percolation transition (e.g. Shandarin et al. 2004). We will discuss this further below. The void volume fraction is shown in the right-hand panels of Figs 4–6 for the Gaussian field and N-body simulations.

4 GAUSSIAN DENSITY FIELD

We first briefly discuss voids in the case of a Gaussian density field. As a cosmologically relevant example of such a field, we consider the initial particle density field used for the N-body simulations. The code generating the initial conditions was used to obtain 10 realizations of a Gaussian field at the stage when $\sigma_\delta \equiv \langle\delta^2\rangle^{1/2} = 0.0155$ (after smoothing at comoving $R_\mathrm{f} = 1\,h^{-1}$ Mpc), which corresponds to an initial field at redshift $z = 150$.

We first discuss the mean void function from the 10 simulations. This is displayed in the left-hand panels of Fig. 1. The top panel shows the monotonic growth of the void function with increase of the void FF from FF = 1 per cent (lowest curve) to FF = 3, 5, 7 and 9 per cent (top curves) before the onset of percolation. The growth stops approximately at FF = 10 per cent as shown in the middle panel. This corresponds to the percolation transition: the merging of voids results in the formation of a percolating network in the underdense phase. After the onset of percolation, the void volume function of isolated voids monotonically decreases with increase in the filling factor: the curves in the bottom panel correspond to FF = 12, 17 and 25 per cent (from top to bottom).

A robust general scaling relation from percolation studies can now be applied to our results. According to this relation (Stauffer & Aharony 1992), the number of large voids scales as

$$n(V) \propto V^{-\tau} \exp(-cV), \tag{3}$$

where $c \propto |\ \mathrm{FF} - \mathrm{FF_c}\ |^{1/\sigma}$; FF $<$ FF$_\mathrm{c}$ where FF$_\mathrm{c}$ is the FF at the percolation transition, and σ and τ are real parameters. Our results for Gaussian fields are seen to be in basic agreement with the percolation model with $\tau \approx 1.95$ as shown by the dashed straight line in Fig. 1: at percolation, the void volume function is well described by a power law over three orders of magnitude. Voids with volumes in the range of the scaling part of the void volume function would be referred to as 'critical clusters'[3] in percolation theory because the power-law behaviour is characteristic of critical phenomena and the properties of these voids are dominated by the behaviour at FF$_\mathrm{c}$. The larger voids in the exponential tail of the void volume function (cf. equation 3) are rare and their properties are not controlled by the system behaviour at FF$_\mathrm{c}$. The scaling properties of the excursion sets in Gaussian and especially non-linear fields are interesting topics and deserve a more detailed study; however they are beyond the scope of the current work. We will return to these issues in the future work.

[3] In percolation theory, the term 'cluster' refers to a group of neighbouring sites satisfying a criterion such as 'occupied' or 'spin-up', etc. In our case, this criterion is set by the density threshold δ_c.

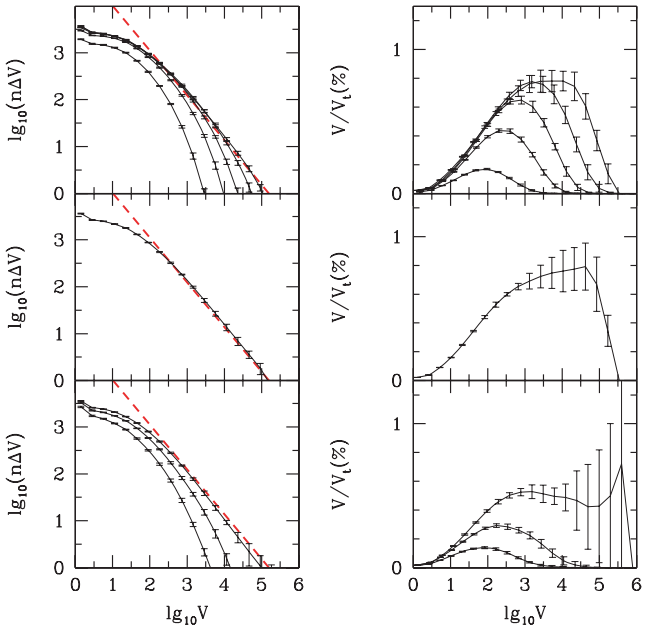

Figure 1. Gaussian field: $\sigma_\delta \approx 0.0155$. The panels on the left-hand side show the void volume function and on the right-hand side the void volume fraction for different FF. The top panels show both the functions before the onset of percolation: FF = 1, 3, 5, 7 and 9 per cent (from bottom to top). The bottom panels show the curves after the onset of percolation: FF = 12, 17 and 25 per cent (from top to bottom). The panels in the middle approximately correspond to the percolation transition; the curves correspond to FF$_\mathrm{c}$ = 10 per cent ($\delta_\mathrm{c} = -0.02$). The mean and the error bars have been derived from 10 realizations of the initial conditions. The dashed straight line in the left-hand panels shows the power law $n\Delta V = 8.9 \times 10^4 V^{-0.95}$, where volume V is measured in $(h^{-1}$ Mpc$)^3$ and $\Delta V/V = 1/\sqrt{2}$.

The volume fraction is shown for the corresponding FF in the right-hand panels of Fig. 1. The basic behaviour of the volume fraction is similar to that of the void function. The volume fraction grows monotonically as the FF is increased until the onset of percolation (right top panel), after which it monotonically decreases (right bottom panel). The onset of percolation is analogous to a phase transition and therefore, due to the expected increase in fluctuations near a 'phase change', it is not surprising that the error bars are significantly greater in the vicinity of FF$_\mathrm{c}$. Although the statistical mean for the percolation transition is FF$_\mathrm{c}$ = 10 per cent, this number will change from realization to realization. When analysing a particular realization, the percolation threshold for the particular realization should be used rather than the statistical mean value. As a consequence of this, somewhat different values for the percolation threshold than given in this section will be encountered in the following analysis. The difference is small, ∼0.5–1 per cent, well inside the 1σ range.

5 VOIDS IN N-BODY SIMULATIONS

In this section, we present a comparative analysis of voids in the initial ($z = 50$) and final ($z = 0$) density fields taken from the N-body simulation. This analysis is targeted at establishing which properties of voids are inherited and which are acquired in the course of evolution. Fig. 2 relates the filling factor to the density contrast. As

Downloaded from https://academic.oup.com/mnras/article-abstract/367/4/1629/1747190/ by guest on 07 October 2019

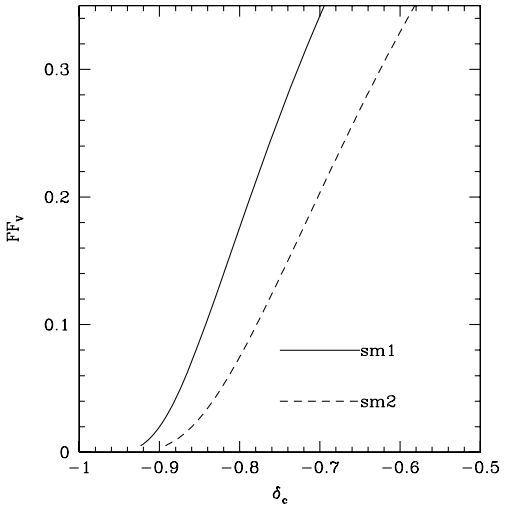

Figure 2. Void filling factor, FF_v, versus density contrast threshold δ_c at $z = 0$ for two smoothing scales: sm1 and sm2 corresponding to $R_f = 1$ and $2\,h^{-1}$ Mpc, respectively. The smallest filling factor is 1 per cent and the largest 35 per cent.

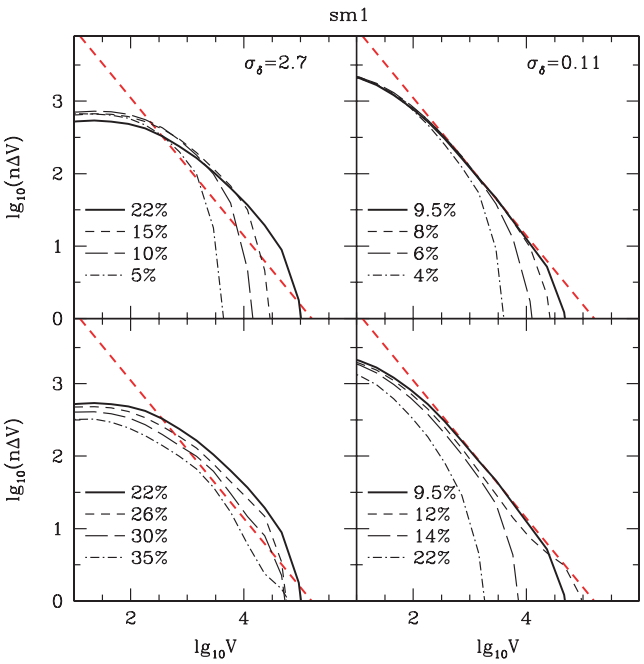

Figure 3. Void volume function $n(V)\Delta V$ with the density field smoothed at $R_f = 1\,h^{-1}$ Mpc. The panels on the left-hand side are for $z = 0$ and on the right-hand side, for $z = 50$. The top panels show the void volume functions at small filling factors before percolation occurs ($FF_c = 22$ per cent, $\delta_c = -0.78$ at $z = 0$ and $FF_c = 9.5$ per cent, $\delta_c = -0.14$ at $z = 50$) and the bottom panels after percolation. The heavy solid lines in the top and bottom panels are the same; they show the void volume function approximately at percolation. The dashed straight line is the same as in Fig. 4, i.e. the power law $n\Delta V = 8.9 \times 10^4 V^{-0.95}$ characteristic of the initial Gausssian density field. Volume V is given in $(h^{-1}$ Mpc$)^3$.

we will see later, the percolation thresholds at $z = 0$ incidentally are close to $\delta = -0.8$ (-0.78 and -0.75 for $R_f = 1\,h^{-1}$ Mpc and $R_f = 2\,h^{-1}$ Mpc, respectively) corresponding to the density contrast of the spherically symmetric top-hat void model when it reaches the first shell crossing. At these thresholds, about a half of the volume of the underdense excursion set is already in one percolating void.

It has been demonstrated in previous studies (Shandarin et al. 2004) that the void volume function is dominated by small voids. This is not surprising at the linear stage of evolution of the density field when the field is essentially Gaussian, but it is also true in the non-linear regime. This is illustrated by Figs 3 and 4 that show the void volume function at different FF and smoothing scales. In these figures, results are shown for the same underlying density field but with different Gaussian filtering windows, $R_f = 1$ and $2\,h^{-1}$ Mpc, respectively.[4]

In Figs 3–4, the two panels on the left-hand side show the number of voids at $z = 0$ while the two panels on the right-hand side represent the initial density field at $z = 50$. The top panels show the void volume functions at several FF corresponding to relatively low-density thresholds when voids do not percolate. The bottom panels are complementary to the top panels and show the void volume function at the thresholds *after* percolation. The heavy solid lines are the same in the top and bottom panels and show the void volume function approximately at the percolation thresholds. These thresholds correspond to a filling factor, FF = 9–9.5 per cent, for the linear fields regardless of the smoothing scale, and decreases from 22 per cent at the smallest smoothing scale ($R_f = 1\,h^{-1}$ Mpc) to 14 per cent at $R_f = 2\,h^{-1}$ Mpc for the evolved field. The dashed straight line is the power law obtained previously for a Gaussian field with the same cosmological parameters.

Fig. 3 clearly demonstrates that the evolution results in a decrease of the number of small voids and an increase in the number of large voids, with the approximate transition boundary between the two behaviours at $V \sim 300\,h^{-3}$ Mpc^3. The field smoothed with $R_f = 2\,h^{-1}$ Mpc (Fig. 4) yields qualitatively similar results; however, there are some quantitative differences. Relative to the $R_f = 1\,h^{-1}$ Mpc smoothing, the number of small voids is lower in both the initial and the final fields, as well as the number of large voids. The former is not unexpected because smoothing with greater scale erases smallest voids. However, the latter result seems to be less obvious since the smoothing scale is relatively small and seemed not to influence large voids. Probably, the explanation is in the significant reduction of the percolation FF in more smoothed density field that makes voids less isolated. As a result, they merge into the percolating voids before they reach large volumes.

The void volume function at the fully developed non-linear stage $z = 0$ is clearly not a power law, while the initial field ($z = 50$) is mostly in good agreement with the scaling discussed in the previous section. The lack of the scaling (power law) component in the void volume function at the non-linear stage is a possible indicator of the presence of large-scale coherence in the density field. This issue will be addressed elsewhere.

In agreement with the Gaussian case, the results displayed in Figs 3 and 4 show that the number of voids monotonically increases with the FF and reaches a maximum at the percolation threshold (top panels), then monotonically decreases with the FF (bottom panels). We conclude that the largest number of voids – practically of every volume – is reached approximately at the percolation thresholds. Below, we show that a small number of the largest voids make up most of the volume of the void excursion set while the majority of voids have very small volumes and constitute only a small fraction of the void excursion set. This is true for all FF at all smoothing scales (Shandarin et al. 2004).

[4] We also have analysed the fields smoothed with $R_f = 4\,h^{-1}$ Mpc, but do not show the results here because they do not reveal anything significant.

Downloaded from https://academic.oup.com/mnras/article-abstract/367/4/1629/1747190/ by guest on 07 October 2019

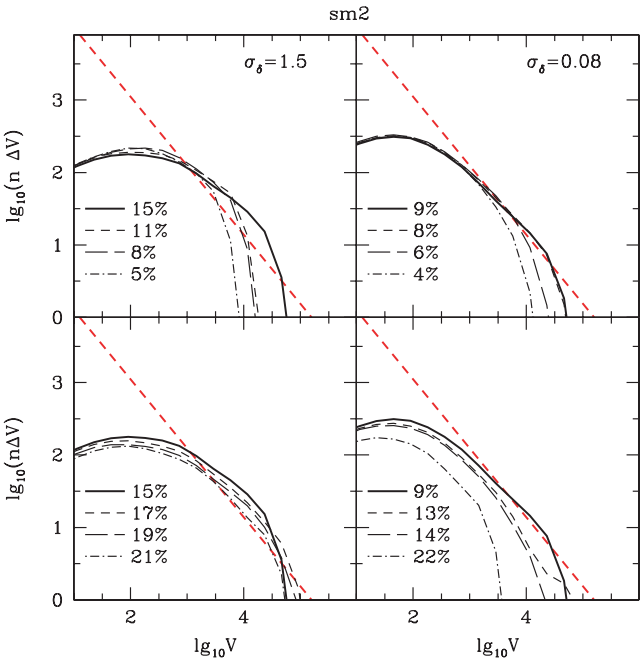

Figure 4. Void volume function $n(V)\Delta V$ with the density field smoothed at $R_{\rm f} = 2\,h^{-1}$ Mpc. The critical parameters are $\mathrm{FF_c} = 15$ per cent, $\delta_{\rm c} = -0.75$ at $z = 0$ and $\mathrm{FF_c} = 9$ per cent, $\delta_{\rm c} = -0.10$ at $z = 50$. The organization of the figure is the same as in Fig. 3. Volume V is given in $(h^{-1}\ \mathrm{Mpc})^3$.

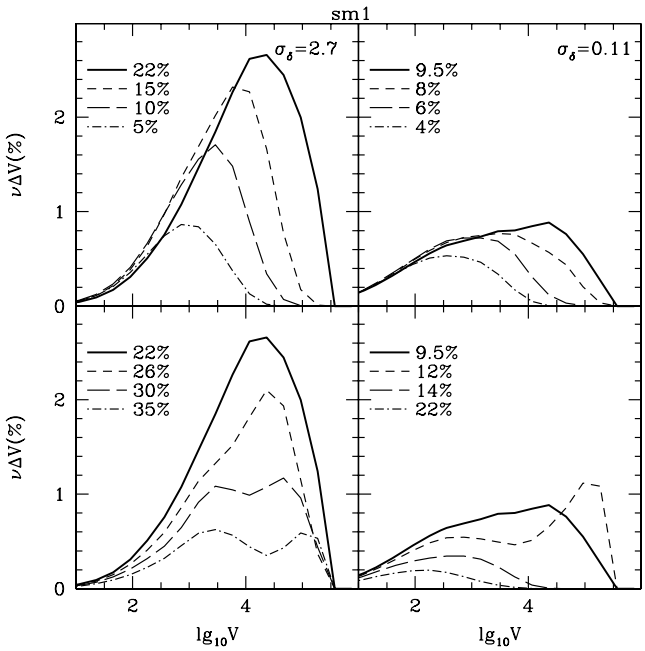

Figure 5. Void volume fraction $v(V)\ \Delta V$ with density field smoothing of $R_{\rm f} = 1\,h^{-1}$ Mpc, following Fig. 3. Volume V is given in $(h^{-1}\ \mathrm{Mpc})^3$.

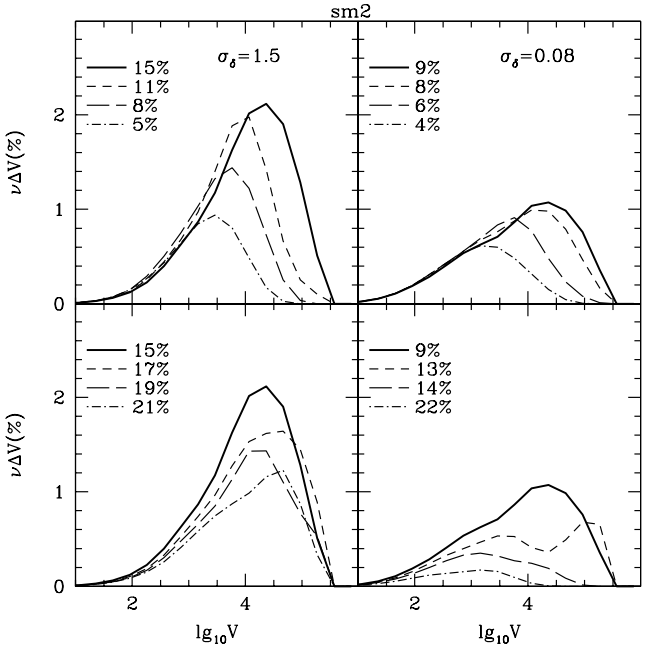

Figure 6. Void volume fraction $v(V)\Delta V$ with density smoothing scale of $R_{\rm f} = 2\,h^{-1}$ Mpc, following Fig. 4. Volume V is given in $(h^{-1}\ \mathrm{Mpc})^3$.

Figs 5 and 6 demonstrate – in a manner similar to the void volume function (Figs 3–4) – that the void volume fraction grows monotonically with the FF until it reaches the percolation threshold shown by the heavy solid lines (top panels). Thereafter, it monotonically decreases with the FF (bottom panels). This occurs because the largest void becomes the percolating void and contains most of the volume of the void excursion set. The volume fraction of voids reaches a maximum at the percolation thresholds for both linear and non-linear fields.

Comparing the void volume fraction (Figs 5 and 6) with the void volume function (Figs 3 and 4), we find that a relatively small number (less than roughly $\simeq$10 per cent) of the largest voids [with approximately $V \geqslant 10^3\ (h^{-1}\ \mathrm{Mpc})^3$] make up most (roughly $\sim$90 per cent or even more) of the void excursion set (see also Shandarin et al. 2004). In their numbers small voids dominate, but they do not contribute significantly to the entire volume of the void excursion set.

The results of this section are summarized in Fig. 7. The top panels show the void volume functions, middle panels, the volume fraction, and bottom panels, the cumulative volume fraction at the percolation thresholds, respectively. Solid lines correspond to the filtering scale $R_{\rm f} = 1\,h^{-1}$ Mpc and dashed lines to $R_{\rm f} = 2\,h^{-1}$ Mpc. We conclude that the percolation threshold is a natural choice characterized by the largest numbers of voids as well as the largest volume fraction in the void excursion set (compare to Shandarin et al. 2004). As mentioned already, a not completely obvious result is that smoothing the density field reduces the number of large voids along with the expected reduction of the number of small voids. It appears that this effect is smaller or even absent in Gaussian fields; however, this may be a statistical fluctuation due to insufficient statistics.

The major effect of the non-linear evolution is summarized in Fig. 8 where the ratio of the number of voids in the N-body simulations to the number of voids in the initial density field at $z = 50$ is plotted as a function of void volume. Voids smaller than $10^3\ (h^{-1}\ \mathrm{Mpc})^3$ are strongly suppressed while voids with greater volumes become approximately three times more abundant than in the parent density field. As a result, the voids smaller than roughly $10^3 (h^{-1}\ \mathrm{Mpc})^3$ comprise less than $\sim$10 per cent of the void excursion set (the bottom panels of Fig. 7). Consequently, we concentrate mostly on larger voids in our further analysis. A somewhat counter-intuitive result is that very large voids [$V > 3 \times 10^5\ (h^{-1}\ \mathrm{Mpc})^3$] are apparently not more abundant at the non-linear stage than in the

Downloaded from https://academic.oup.com/mnras/article-abstract/367/4/1629/1747190/ by guest on 07 October 2019

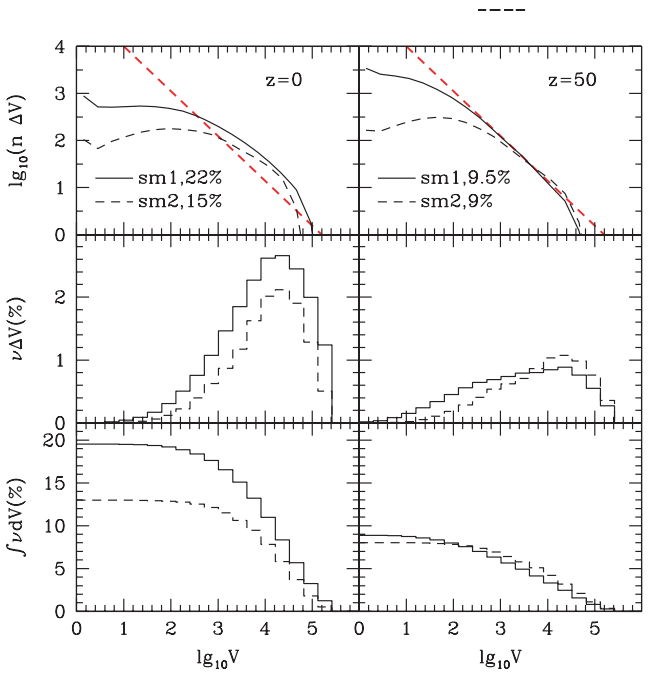

Figure 7. Summary of the information in Figs 3–6; the volume functions and volume fractions are shown at the corresponding percolation thresholds. Top: the volume functions at $z = 0$ (left-hand side) $z = 50$ (right-hand side). Middle: the corresponding volume fractions. Bottom: the cumulative void fractions: $\int_V^\infty v\,dV$. Volume V is given in $(h^{-1}\ \mathrm{Mpc})^3$.

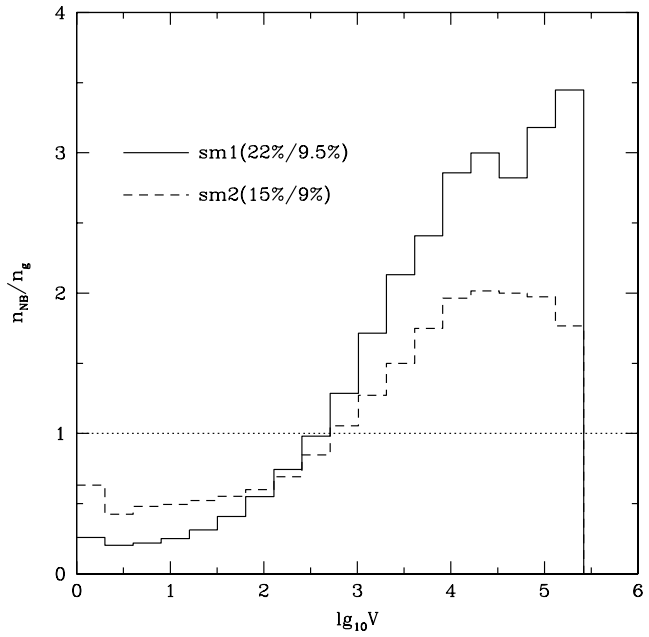

Figure 8. Ratio of the number of voids in the N-body simulations to the number of voids in the initial density field at $z = 50$ as a function of volume. The voids were identified at the corresponding percolation thresholds in every density field: for N-body simulation at FF = 22 and 15 per cent at $R_\mathrm{f} = 1$ and $2\,h^{-1}$ Mpc, respectively, and for initial state at FF = 9.5 and 9 per cent at these smoothing scales, respectively. Volume V is given in $(h^{-1}$ Mpc$)^3$.

initial density field; this could be an artefact due to the finite size of the simulation box, however, and should be checked using larger volume simulations.

We now discuss how the excursion set definition of voids – as regions bound by isodensity surfaces – results in seeming disagreement with other definitions of voids. Most significantly, we find that the amount of space in isolated voids is not large. For a smoothing scale of $R_\mathrm{f} = 1\,h^{-1}$ Mpc, it is only about 20 per cent of all space, and for $R_\mathrm{f} = 2\,h^{-1}$ Mpc it is even less: about 15 per cent. In contrast, other studies would claim that most of space is taken up by voids. This discrepancy is rather easy to explain: we deal with isolated voids naturally defined by isodensity surfaces, while in other studies voids are built using procedures that follow the density contours only approximately, thereby allowing the closure of the boundaries of the constructed voids by non-isodensity surfaces. With our definition of voids, one can get as much of void space as one wants by raising the density threshold, but then the natural isodensity surfaces would inevitably build a single void percolating throughout the entire volume plus a few small isolated voids. Cutting the percolating void into pieces would finish the job of constructing large 'isolated' voids; however this brings a certain arbitrariness, and therefore bias, into the analysis. Other algorithms actually suggest various methods of doing this, but without explicit discussion. Our procedure does not cut the largest void – neither before nor after it percolates – and therefore the voids found by it can make up only a relatively small fraction of space. At even greater density thresholds, the percolating void is absolutely dominant (Shandarin et al. 2004). Reducing the smoothing scale increases the number of voids and the amount of space occupied by isolated voids (Fig. 7). However, if a uniform filter is used for smoothing, then the intrinsic discreetness of N-body simulations takes over and prevents further reduction of the smoothing scale. An adaptive smoothing filter would help to ameliorate this problem.

6 FITTING TO ELLIPSOIDS

As discussed in Introduction, the actual shapes of voids are often taken to be approximately spherical or ellipsoidal. In order to investigate possible systematic difficulties with this kind of fitting, we identify all voids at a selected density threshold (roughly at the percolation threshold) and then fit each void by an ellipsoid having the same inertia tensor as the void itself:

$$J_{xx} = \sum_i m_i \left(y_i^2 + z_i^2\right), \qquad J_{xy} = -\sum_i m_i x_i y_i, \qquad \text{plus cyclic permutations,} \tag{4}$$

where m_i and x_i, y_i, z_i are the mass and coordinates of the site with respect to the void centre of mass, and the sum is taken over all sites belonging to the void. The semi-axes of the fitting ellipse can be found from the principal moments of inertia J_1, J_2, J_3, viz,

$$a^2 = \frac{5}{2M}(J_2 + J_3 - J_1) \qquad \text{plus cyclic permutations,} \tag{5}$$

where $M = \sum m_i$ is the mass of the void. Our focus here is on the geometrical properties of voids and therefore we compute the inertia tensor of an empty void by setting all the m_i to a constant. We reserve the study of another interesting option, where the m_i are actual dark matter masses in the grid cells, for future work. Fig. 9 illustrates the fitting procedure outlined above for two example voids: in the figure, the voids are shown on the left-hand side with the corresponding ellipsoids on the right-hand side. The axes of the fitting ellipsoid, $a > b > c$, can be used to evaluate the volume of the ellipsoid $V_\mathrm{E} = (4\pi/3)abc$ as well as the ratios b/a and c/b which approximately characterize the shape of the void. The Planarity $P = (1 - b/a)/(1 + b/a)$ and Filamentarity $F = (1 - c/b)/(1 + c/b)$

Downloaded from https://academic.oup.com/mnras/article-abstract/367/4/1629/1747190/ by guest on 07 October 2019

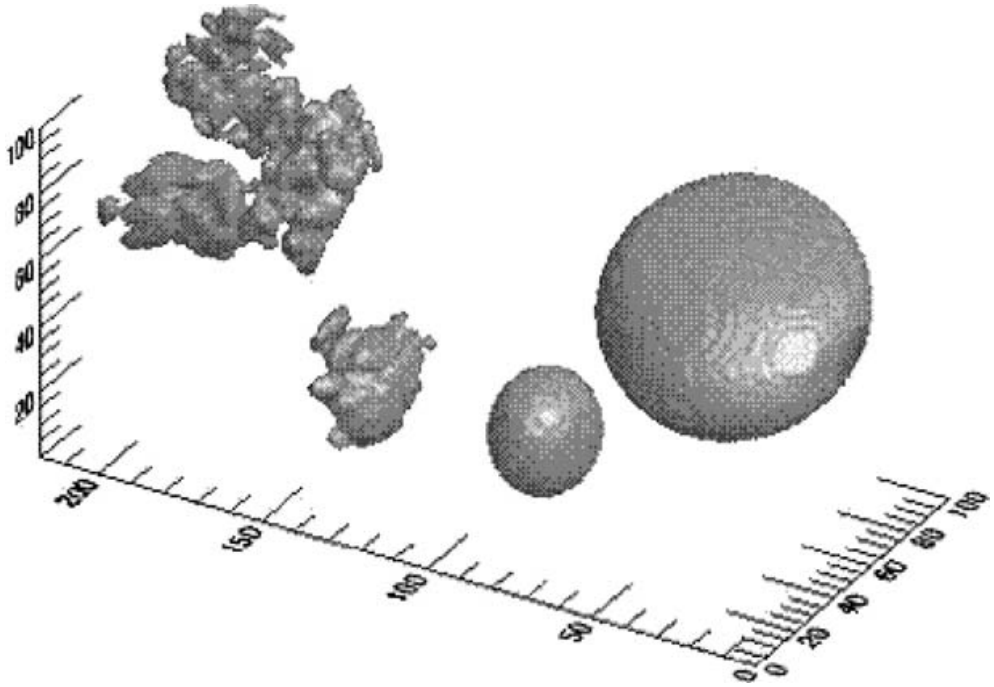

Figure 9. Comparison of an ellipsoid fit to high- and low-porosity voids. The low-porosity small void (bottom left) has volume of $V = 7500$ $(h^{-1}$ Mpc$)^3$. Porosity $P = V_{\rm E}/V_{\rm V} = 1.92$, and Inverse Porosity IP $= V_{\rm V}/V_{\rm E} = 0.52$; the fitting ellipsoid is at the bottom right. The high-porosity large void (top left) has volume of $V = 24\,000$ cells, P $= 4.72$ and IP $= 0.21$. The axes are in h^{-1} Mpc.

(Sahni, Sathyaprakash & Shandarin 1998; Shandarin et al. 2004) are equivalent measures of void shape.

If a void is ideally ellipsoidal, then its volume must equal that of the fitting ellipsoid. Actual voids are not ellipsoidal in shape, however (Fig. 9), thus their volumes $V_{\rm V}$ are always smaller than the volumes of the fitting ellipsoids $V_{\rm E}$. The ratio $P = V_{\rm E}/V_{\rm V}$ – dubbed the Porosity – quantifies the quality of the ellipsoidal fit. We use the Inverse Porosity IP $= V_{\rm V}/V_{\rm E} (0 \leqslant {\rm IP} \leqslant 1)$ as a simple estimate of the goodness of the ellipsoidal fit. If IP is close to unity, the fit may be regarded as good, otherwise the smaller the IP, the worse the fit.

7 SPHERICITY

Deforming a sphere into an ellipsoid with three axes, $a \geqslant b \geqslant c$, one obtains a two-parameter family of shapes that can be fully characterized by two ratios: b/a and c/b. Nevertheless, we would like to approximately describe the departure from a sphere with only one parameter. Ideally, the parameter should have a simple geometric interpretation and only a small variation when the remaining degree of freedom is varied. We suggest the use of the ratio of the smallest to largest axis, $\alpha = c/a$, for this purpose. Using this, one can distinguish three archetypal shapes among the entire two-parameter family characterized by α: pancake-like with $b/a = 1$ and $c/b = \alpha$, filament-like with $b/a = \alpha$ and $c/b = 1$, and ribbon-like with $b/a = c/b = \sqrt{\alpha}$. All three have very distinct limits at $\alpha \to 0$. Fig. 10 provides a visual illustration of the variation of shapes from a pancake through a ribbon to a filament for three values of α.

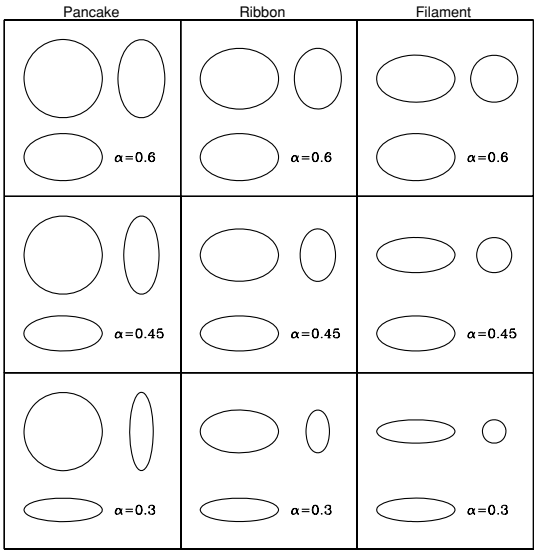

Figure 10. Three principal projections of an ellipse are shown in every panel. Each column shows one of three archetypes of the deformed sphere parametrized by one number $\alpha = c/a$ $(0 \leqslant \alpha \leqslant 1)$: pancake-like ($b/a = 1$, $c/b = \alpha$), ribbon-like ($b/a = \sqrt{\alpha}$, $c/b = \sqrt{\alpha}$) and filament-like ($b/a = \alpha$, $c/b = 1$).

8 SHAPES OF VOIDS IN *N*-BODY SIMULATIONS

In this section, we discuss the shapes of voids in the simulated ΛCDM model at the present epoch ($z = 0$). As earlier, we analyse the density distribution in real space at three different smoothing scales: 1, 2 and 4 h^{-1} Mpc.

8.1 Mean values

The mean Sphericity as a function of the volume is shown in Fig. 11. Every line shows the ratio at a different FF and for all three smooth-

Downloaded from https://academic.oup.com/mnras/article-abstract/367/4/1629/1747190/ by guest on 07 October 2019

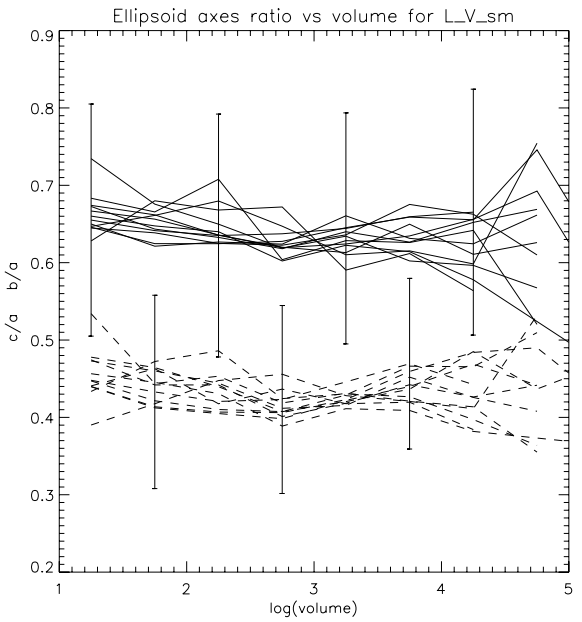

Figure 11. Axis ratios as a function of volume. The average of the axis ratios is independent of the filling factor and smoothing length. Except for very small voids, the average is constant with volume. Volume V is given in $(h^{-1}\ \mathrm{Mpc})^3$.

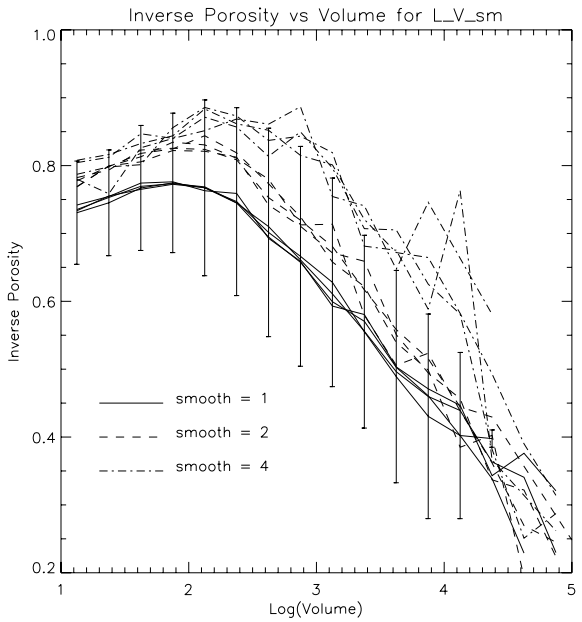

Figure 12. Inverse Porosity (IP $= V/V_\ell$) as a function of void volume. The larger the volume, the larger is the Porosity on average. There is little dependence on the filling factor, while the smoothing length systematically suppresses the Porosity. Volume V is given in $(h^{-1}\ \mathrm{Mpc})^3$.

ing scales. The variance is shown by vertical bars for one of the lines, the others being very similar. It is clear that there is no significant statistical difference between the mean shapes of voids at different filling factors or smoothing scale: on average $b/a \approx 0.65$ and $c/a \approx 0.45$. Thus, if a region of the underdense excursion set is approximated by an ellipsoid, then the ellipsoid should be triaxial with the shortest axes at least twice shorter than the longest one. A substantial number of ellipsoids have shortest axes as small as a third of the longest one. Fig. 10 provides the visual illustration of such ellipsoids.

In Fig. 12, we illustrate the dependence of the mean Inverse Porosity IP $= V_{\mathrm{V}}/V_{\mathrm{E}}$ as a function of the volume of the void for different FF and smoothing scales. Following the behaviour of the Sphericity, the Porosity does not show a strong dependence on the FF; however there are two other characteristics that are very different from the mean Sphericity. The first is a systematic growth of the mean Inverse Porosity with the smoothing length, albeit with large variance. This is an obvious consequence of smoothing; the voids in the smoothed density fields being more ellipsoidal. The other is a clear dependence on the volume of the voids: the larger the volume, the smaller the Inverse Porosity, and therefore the worse the ellipsoidal fit. Combining the information in Figs 12 and 7, we conclude that large voids $V > 3 \times 10^3\, h^{-1}\ \mathrm{Mpc}^3$ – making most of the void excursion set – cannot generically be adequately approximated by ellipsoids.

8.2 Distribution functions

Statistical information regarding the quality of elliptical and spherical void fits can be gleaned from the distribution functions for the Inverse Porosity and the Sphericity. We begin by first discussing the Inverse Porosity distribution function. Figs 13 and 14 show the IP distribution for density fields smoothed on three scales: $R_{\mathrm{f}} = 1\, h^{-1}\ \mathrm{Mpc}$ (solid line), $R_{\mathrm{f}} = 2\, h^{-1}\ \mathrm{Mpc}$ (short-dashed line) and $R_{\mathrm{f}} = 4\, h^{-1}\ \mathrm{Mpc}$ (long-dashed line). Fig. 13 includes all the voids with volume greater than $10(\, h^{-1}\ \mathrm{Mpc})^3$ and Fig. 14 with volume greater than $1000(\, h^{-1}\ \mathrm{Mpc})^3$. The first cut is imposed because the shape measurement of small voids $V < 10\ (\, h^{-1}\ \mathrm{Mpc})^3$ is not reliable. The second cut selects only large voids $V > 1000(\, h^{-1}\ \mathrm{Mpc})^3$ comprising approximately 90 per cent of the void excursion set (cf. Fig. 7). If voids with $V < 1000\ (\, h^{-1}\ \mathrm{Mpc})^3$ are included, the IP distribution peaks relatively close to unity, implying that elliptical fits are quite good for the majority of the voids. As we demonstrated earlier, however, small voids dominate only in number and not in volume. If small voids are excluded (Fig. 14), then the IP distribution peaks at $V_{\mathrm{V}}/V_{\mathrm{E}} \approx 0.45$ for $R_{\mathrm{f}} = 1$ and $R_{\mathrm{f}} = 2\, h^{-1}$ Mpc. In this case, the ellipsoidal fit is quite poor for most of the larger voids that make up roughly 90 per cent of the void excursion set. Therefore, in the following analysis we will exclude voids with volumes less than $1000\ (\, h^{-1}\ \mathrm{Mpc})^3$.

We note that the IP distribution in Fig. 14 displays a trend of the distribution peak shift to the right with increased smoothing scale, with an especially pronounced change for $R_{\mathrm{f}} = 4\, h^{-1}$ Mpc. This is expected as smoothing will improve the ellipsoidal fit for the smallest voids considered; for $R_{\mathrm{f}} = 4\, h^{-1}$ Mpc, a sphere with the radius of the smoothing length has a volume of $270\ (\, h^{-1}\ \mathrm{Mpc})^3$ which is more than one quarter of the volume of the smallest voids that dominate the void number distribution.

Turning to the Sphericity, Fig. 15 shows the Sphericity distribution function for large voids $V_{\mathrm{V}} > 1000\ (\, h^{-1}\ \mathrm{Mpc})^3$. In this case, the results from fields smoothed on different scales are not very different. The mean Sphericity of the fitting ellipsoids is about 0.45 (in agreement with Fig. 11). The middle panels of Fig. 10 show three archetypal ellipsoids corresponding to this value. The top and bottom panels show the range of Sphericity for most of the voids.

9 SUMMARY AND DISCUSSION

In this paper, we studied the distribution of underdense regions (voids) in N-body simulations for the ΛCDM model, voids being

Downloaded from https://academic.oup.com/mnras/article-abstract/367/4/1629/1747190/ by guest on 07 October 2019

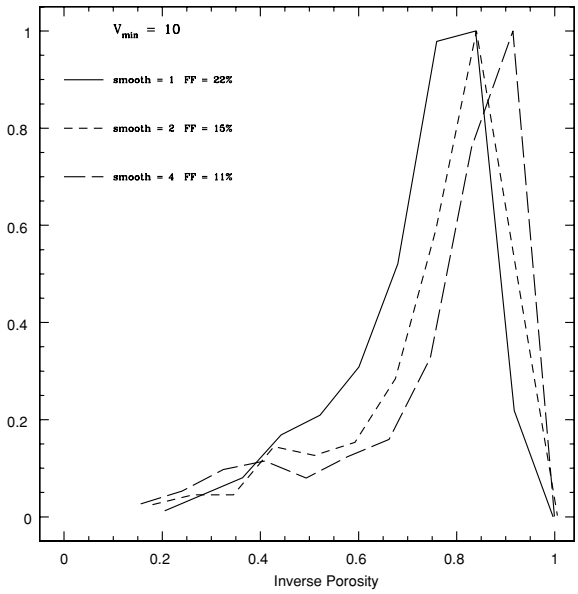

Figure 13. Normalized distribution functions of the Inverse Porosity ($V_{\rm V}/V_{\rm E}$) of voids with volumes $V_{\rm V} > 10\,(h^{-1}\,{\rm Mpc})^3$ at three smoothing scales. The distribution functions are shown for the corresponding percolation thresholds.

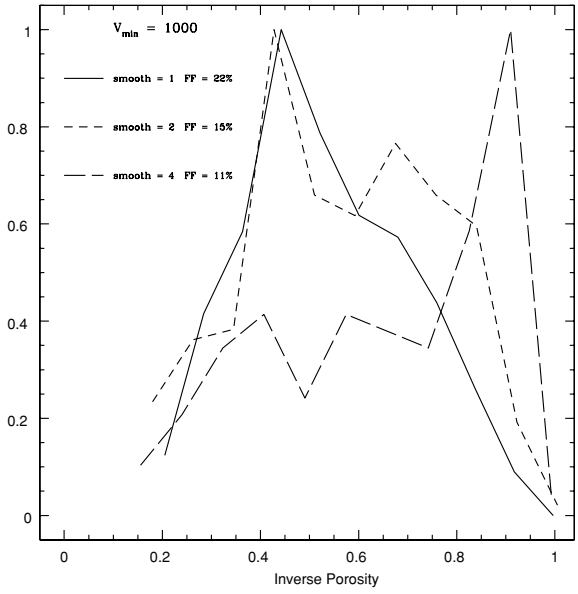

Figure 14. Normalized distribution function of the Inverse Porosity ($V_{\rm V}/V_{\rm E}$) of voids with volumes $V_{\rm V} > 1000\,(h^{-1}\,{\rm Mpc})^3$ at three smoothing scales following Fig. 13.

defined as individual regions of the underdense excursion set: $\delta < \delta_{\rm c}$. In practice, we additionally applied the neighbour-of-neighbour criterion for grid sites satisfying the above threshold condition. By defining the void volume function, we then showed that the largest number of voids of any size is reached just before the onset of percolation. In other words, as the density threshold is increased, more and more voids are found and the total volume fraction in voids increases; this continues up to a critical point beyond which the number of voids and the volume fraction in all but the percolating void begin to decrease.

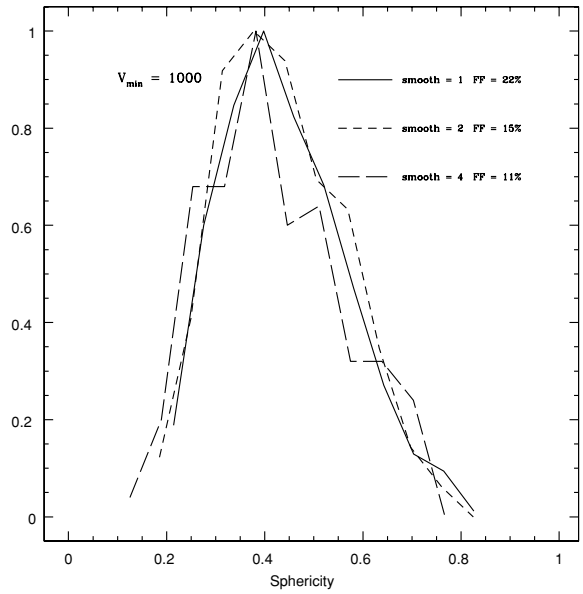

Figure 15. Sphericity distribution function of voids with volumes $V_{\rm V} > 1000\,(h^{-1}\,{\rm Mpc})^3$ at three smoothing scales. The distribution functions are shown for the corresponding percolation thresholds.

The percolation transition motivates a particular density threshold and corresponding FF to focus on further analysis, i.e. the percolation threshold itself. After percolation, though the volume of the underdense excursion set continues monotonically to increase with the growth of the density threshold, the number and volume of individual voids decrease because merging of individual voids into the single percolating void dominates. The percolating void continues to grow monotonically with the threshold, mostly by absorbing individual voids. Choosing a particular threshold above the percolation point seems to be arbitrary in most cases and may significantly affect the results one obtains.

One could cut the percolating void found at an arbitrary threshold into pieces. But without any clear physical motivation, this would introduce an additional arbitrariness which we wished to avoid. It should also be noted that special precaution should be exercised in one's notion of a void, as it is always possible to design an algorithm producing more or less spherical voids if so desired. The guideline provided by Icke (1984) suggesting that voids become more spherical in the course of dynamical evolution should be reconsidered in a more realistic environment rather than in the case of a single void placed in a homogeneous universe. The external shear is likely to play an important role (Eisenstein & Loeb 1995) and must be included in the model. Even in the case of a single void, the effect may be quantitatively insufficient (Bertschinger 1985). We will address these issues in future work.

As a cautionary note, we stress that the reported results may depend on the resolution of simulations, smoothing procedure adopted here and the values of the filtering scale. This is an issue with essentially all proposed definitions of voids and needs to be further investigated.

The density field at an early enough epoch is essentially Gaussian random on scales below the smoothing scales employed here. We considered 10 realizations of a density field at $z = 150$ and showed that the behaviour of the void volume function closely followed a mathematical form motivated by percolation theory; at later redshifts, the field is no longer Gaussian and this form does not hold.

Downloaded from https://academic.oup.com/mnras/article-abstract/367/4/1629/1747190/ by guest on 07 October 2019

At the present epoch, we found that less than 10 per cent or so of the largest voids, with volumes greater than about 10^3 $(h^{-1}\,\mathrm{Mpc})^3$, hold more than 90 per cent of the void excursion set while small voids dominate in their numbers. The dynamic evolution of voids results in a significant decrease in the number of small voids [$V < 10^3$ $(h^{-1}\,\mathrm{Mpc})^3$] and an increase in the number of large voids.

In order to study effective void shapes, we fit the underdense regions to ellipsoids with the same inertia tensor as the voids. We used this to define the Sphericity and (Inverse) Porosity of the voids and showed that most large voids are not spherical and have irregular geometries which lead to high porosity (low Inverse Porosity). The prevailing assumption of spherical voids, used extensively in the literature, is not a good approximation if the actual isodensity surfaces are employed as the void boundaries. We found that the ratios of the semimajor axes have mean values of 0.65 and 0.45 and the Sphericity has a mean value of $c/a \approx 0.45$, (where c and a are the smallest and the largest semi-axes of the fitting ellipsoids), which is clearly not spherical. In addition, the Porosity measure showed that large voids are quite porous whereas small voids are more regular, with even ellipsoidal fitting becoming problematic for the larger voids.

Two questions are of potential relevance here. First, the representing ellipsoid has the same inertia tensor as a homogeneous void while actual voids are inhomogeneous. Therefore, one could ask: would the true density profile change the fitting ellipsoid to be closer to a sphere? The obvious answer is no; it is natural to expect the central part of a void to be more spherical than the boundary region, but this would have a smaller effect on the inertia tensor since the density at the centre of the void is lower than near the boundary.

The second question relates to the shapes of voids before the onset of percolation. Is it possible that the percolating void has the shape of a set of spheres connected by narrow tunnels – one of the major concerns of Kauffmann & Fairall (1991) and El-Ad & Piran (1997)? This appears unlikely because the percolating void is made by the merger of individual voids as the density threshold is increased. The merger process happens quite quickly near the threshold (i.e. with a small change of the threshold), therefore the individual voids making up the percolating void cannot change their shapes appreciably. Our results show that the largest of them are neither spherical nor even elliptical. Additionally, study of individual voids before and after percolation does not show much difference in volumes and shapes (Shandarin et al. 2004).

ACKNOWLEDGMENTS

SH and KH acknowledge support from the Department of Energy via the LDRD program of Los Alamos National Laboratory. The calculations described herein were performed primarily using the computational resources of Los Alamos National Laboratory. A special acknowledgment is due to supercomputing time awarded to us under the LANL Institutional Computing Initiative. This research is supported by the Department of Energy, under contract W-7405-ENG-36. HAF was supported in part by the GRF at the University of Kansas. SS was partly supported by NSF-RP087 grant. SS also acknowledges the support from 'Non-linear Cosmology Program' at Observatoire de la Côte d'Azur Nice, Centre de Physique Théorique CNRS Marseille and Institut d'Astropysique de Paris in summer 2005. SS, KH and SH acknowledge support from the Aspen Center for Physics where the manuscript was finalized. We acknowledge useful discussions with Ravi Sheth and especially Rein van de Weygaert whose detailed comments were invaluable.

REFERENCES

Adelman-McCarthy J. K. et al., 2006, ApJS, 162, 38
Aikio J., Mähönen P., 1998, ApJ, 497, 534
Amendola L., Frieman J. A., Waga I., 1999, MNRAS, 309, 465
Benson A. J., Hoyle F., Torres R., Vogeley M., 2003, MNRAS, 340, 160
Bertschinger E., 1985, ApJS, 58, 1
Colberg J. M., Sheth R. K., Diaferio A., Gao L., Yoshida N., 2005, MNRAS, 360, 216
Colless M. M. et al., 2001, MNRAS, 328, 1039
Dubinski J., da Costa L. N., Goldwirth D. S., Lecar M., Piran T., 1993, ApJ, 410, 458
Eisenstein D. J., Loeb A., 1995, ApJ, 439, 520
El-Ad H., Piran T., 1997, ApJ, 491, 421
Goldberg D. M., Vogeley M. S., 2004, ApJ, 605, 1
Gottlöber S., Łokas E. L., Klypin A., Hoffman Y., 2003, MNRAS, 344, 715
Gregory S. A., Thompson L. A., 1978, ApJ, 222, 784
Heitmann K., Ricker P. M., Warren M., Habib S., 2005, ApJS, 160, 28
Hoyle F., Vogeley M. S., 2002, ApJ, 566, 641
Hoyle F., Rojas R. R., Vogeley M. S., Brinkmann J., 2005, ApJ, 620, 618
Icke V., 1984, MNRAS, 206, 1
Jenkins A. R. et al., 1998, ApJ, 499, 20
Kauffmann G., Fairall A. P., 1991, MNRAS, 248, 313
Kirshner R. P., Oemler A., Schechter P. L., Shectman S. A., 1981, ApJ, 248, L57
Klypin A. A., Holtzman J., 1997, preprint (astro-ph/9712217)
Kofman L. A., Pogosyan D., Shandarin S. F., Mellot A. L., 1992, ApJ, 393, 437
Lin C. C., Mestel L., Shu F., 1965, ApJ, 142, 1431
Peebles P. J. E., 2001, ApJ, 557, 495
Peebles P. J. E., 1980, The Large-Scale Structure of the Universe. Princeton Univ. Press, Princeton, NJ
Plionis M., Basilakos S., 2002, MNRAS, 330, 399
Rojas R. R., Vogeley M., Hoyle F., Brinkmann J., 2004, ApJ, 617, 50
Rood H. J., 1988, ARA&A, 26, 245
Ryden B. S., 1995, ApJ, 452, 25
Sahni V., Sathyaprakash B. S., Shandarin S. F., 1994, ApJ, 431, 20
Sahni V., Sathyaprakash B. S., Shandarin S. F., 1998, ApJ, 495, L5
Schaap W. E., van de Weygaret R., 2000, A&A, 363, L29
Shandarin S. F., Sheth J., Sahni V., 2004, MNRAS, 353, 162
Sheth J., Sahni V., Shandarin S. F., Sathyaprakash B., 2003, MNRAS, 343, 22
Sheth R. K., van de Weygaert R., 2004, MNRAS, 350, 517
Slezak E., de Lapparent V., Bijaoui A., 1993, ApJ, 409, 517
Spergel D. N. et al., 2003, ApJS, 148, 175
Stauffer D., Aharony A., 1992, Introduction to Percolation Theory. Taylor & Francis, London
van de Weygaert R., 2002, in Plionis M., Cotsakis S., eds, Proc. 2nd Hellenic Cosmology Workshop, Astrophys. Space Sci. Library Vol. 276. Kluwer, Dordrecht, p. 119
van de Weygaert R., van Kampen E., 1993, MNRAS, 263, 481
Zel'dovich Ya. B., Einasto J., Shandarin S. F., 1982, Nat, 300, 407

APPENDIX A: ESTIMATE OF MATTER FLOW IN VOID FORMATION

We suggest the following simple estimate of the comoving distance travelled by a fluid element in the process of the formation of a spherical void of radius R. We assume (i) the initial density is the mean density, (ii) the final density is uniform in the void and is a fraction $f < 1$ of the mean, (iii) the motion is purely radial and (iv) all the mass is accumulated on an infinitesimally thin shell of radius R.

Downloaded from https://academic.oup.com/mnras/article-abstract/367/4/1629/1747190/ by guest on 07 October 2019

The model is purely kinematic and makes no assumptions regarding the dynamics. It corresponds to the following mapping:

$$r = \begin{cases} q + A\,q \text{ if } q + Aq \leqslant R, & (q \leqslant q_{\rm c}), \\ R \qquad\quad \text{if } q + Aq > R, & (q > q_{\rm c}), \end{cases} \tag{A1}$$

where q and r are the initial and final positions of a fluid element. The amplitude A is determined by the value of f: $A = f^{-1/3} - 1$. The critical value $q_{\rm c}$, where the mapping changes its form, is $q_{\rm c} = R/(1 + A) = f^{1/3}\,R$.

The mean distance travelled by a fluid element is

$$\bar{d} = \frac{3}{4\pi R^3}\left[\int_0^{q_{\rm c}} (Aq) 4\pi q^2\,{\rm d}q + \int_{q_{\rm c}}^{R} (R - q) 4\pi q^2\,{\rm d}q\right] \tag{A2}$$

$$= \frac{1 - f}{4} R, \tag{A3}$$

which obviously understates the actual mean distance due to assumption (iv). The maximum distance travelled by fluid elements is $d_{\rm max} = (1 - f^{1/3})R$. If $f = 0.1$, then $\bar{d} \approx 0.22R$ and $d_{\rm max} \approx 0.54\,R$.

Denoting the fraction of the distance by $\xi = d/R$, one can obtain the probability density function of the distances travelled by the fluid elements

$$\begin{aligned} {\rm d}F &= 3\left\{1 - 2\xi + \left[1 + \frac{f}{(1 - f^{1/3})^3}\right]\xi^2\right\}{\rm d}\xi, \\ &0 \leqslant \xi \leqslant 1 - f^{1/3}. \end{aligned} \tag{A4}$$

This paper has been typeset from a TEX/LATEX file prepared by the author.

Downloaded from https://academic.oup.com/mnras/article-abstract/367/4/1629/1747190/ by guest on 07 October 2019